Effect of Simulated Annealing Conditions on Scale Formation and Neutral Electrolytic Pickling

*Susanna Airaksinen[1)], Teemu Tuovinen[2)], Aleksi Laukka[1)], Tero Vuolio[1)], Eetu-Pekka Heikkinen[1)], Elina Riekki[3)], Timo Manninen[3)], Timo Fabritius[1)]**

[1)] Prof. T. Fabritius, S. Airaksinen, A. Laukka, T. Vuolio, E.-P. Heikkinen
Process Metallurgy Research Unit,
University of Oulu,
P.O. Box 4300, 90014 Oulu, Finland
Email: timo.fabritius@oulu.fi

[2)] T. Tuovinen
Research Unit of Sustainable Chemistry,
University of Oulu, Oulu, Finland

[3)] E. Riekki, T. Manninen
Outokumpu Stainless Oy, Tornio, Finland

Keywords: austenitic stainless steel, annealing, scale formation, electrolytic pickling

Abstract

Scale formation of AISI 304 stainless steel during annealing at temperatures between 1100 and 1200 °C under a water vapor-containing atmosphere was studied. Characterization of the oxide scale was performed with FESEM-EDS and GDOES and removal of oxide scale was done via neutral electrolyte pickling. The pickling conditions were kept constant and the effect of the annealing conditions and scale properties on the pickling result were examined. The effectiveness of pickling was evaluated using analysis FESEM images taken on polished sections of pickled surfaces. Research shows that the thickness, morphology, and composition of the oxide scale are dependent on annealing temperature and time. The thicknesses of the scale formed under the established conditions varied from 0.2 to over 30 µm, and morphologies between the chromium rich oxide layer and layered scale structure formed by breakaway oxidation. The pickling response of oxide scales remained good at all annealing temperatures with the shortest exposure time.

1. Introduction

Stainless steel annealing is part of the steel manufacturing process in an industrial rolling mill. After cold-rolling, the annealing is performed at a high temperature and short exposure time and in an oxidizing atmosphere in a continuous annealing furnace during the process.[1] The purpose of annealing cold-rolled stainless steel is to produce complete recrystallization and proper grain size, which comprise a significantly important basis for the mechanical properties of cold-rolled stainless steel.[2] Annealing produces a thin oxide scale layer on the surface of the strip. The characteristics of this layer are thickness, composition, and morphology, all of which are dependent on the annealing conditions. The type of the oxide scale layer affects the efficiency of the descaling processes after annealing.[3]

High temperature oxidation of types 304 and 304L stainless steels has been studied under various atmospheres and exposure times. Prior studies of long-term oxidations[4-9] focus on the scaling behavior of stainless-steel end-products during oxidizing operating conditions. Habib et al. observed an increase in oxidation due to the breaking of protective oxide layer after 2 h oxidation at 1000 °C.[10] Col et al. studied the development of oxide layer on the surface of AISI 304L during 48-312 h oxidation at 850 °C and resulted in the onset of breakaway oxidation in 110 hours. [11] Parry et al. investigated the effect of cold-rolling on the composition of formed oxide scale after long-term oxidation of AISI 304L at 830 °C. [12]

The effect of short-term oxidation on oxide scale formation has also been investigated previously. Zacchetti et al.[13] observed that oxidation produced a thin protective chromium-rich oxide layer at temperatures above 1000 °C when using enough of an oxygen-containing atmosphere. Gonzales et al.[2] found enrichment of silicon and manganese in the oxide layer using oxidation times of less than five minutes at 1120 °C. de Carvalho et al.[14] studied the

oxidation of AISI 304 at high temperatures for 10 to 30 minutes and reported that the formed oxide consisted mainly of hematite and spinel-like phases.

Researchers have likewise found that the atmosphere influences the formation of oxide scale during the high temperature oxidation of stainless steel.[15-18] Annealing in an oxidizing atmosphere requires at least 2–3 % oxygen to produce a scale that is easier to pickle than scales formed in lower oxygen contents.[19] In a continuous annealing furnace, the combustion of fuel gases produces water vapor, and similar simulated process atmosphere has been used to study oxidation. [20-23] The type of fuel used and the air-fuel ratio affect the water vapor and free oxygen contents in the furnace atmosphere.[1] The formation of a protective and non-protective scale layer on the surface of type AISI 304 stainless steel has been found to be dependent on air/CH_4 ratios due to the fact that protective scale layers formed in free oxygen-containing atmospheres.[1,20] Lindell et al. [24] reported the exchange of propane combustion from air to oxygen, which significantly increases the proportion of water vapor in the atmosphere, does not affect the composition of the oxide scale.

The effects of annealing conditions on the removal of the developed oxide scale have been reported in fewer studies. Fernando et al.[25] performed high temperature annealing of cold-rolled AISI 304 with a maximum of 60-second exposure times with different oxygen contents and found that the effect of annealing conditions on the pickling result depended on the pickling method. Ipek et al.[26] observed a correlation between the effectiveness of neutral electrochemical pickling and a decrease in the mixed acid pickling time. Lindell et al.[3] examined the acid pickling behavior of production line-annealed austenitic grades and found that the cold-rolled type of AISI 304L stainless steel is easier to pickle than AISI 309L.

The objective of this study was to investigate the effects of annealing conditions on oxide scale formation in the final annealing of a cold-rolled AISI 304 strip and on the efficiency of electrolytic descaling.

The objective of this study was to investigate the effects of exceptional industrial annealing conditions on oxide scale formation in the final annealing of a cold-rolled AISI 304 strip and on the efficiency of electrolytic descaling. The exceptional conditions are formed in an industrial furnace as the results of a deviation from normal operation. For example, after production halt of the annealing line, in which case the annealing temperature and thus progression rate of steel strip may differ from ordinary. The morphology, composition, and thickness of the formed scale were determined using field emission scanning electronic microscopy (FESEM), energy dispersive spectroscopy (EDS), and glow discharge optical emission spectroscopy (GDOES). Descaling of the annealed samples was performed by neutral electrolyte pickling, and its effectiveness was estimated based on FESEM image analysis and explanatory data analysis.

2. Experimental

2.1. Materials and Methods

The cold-rolled AISI 304 stainless steel strip samples used in this study were supplied by Outokumpu Stainless. The thickness of the steel sheets cut from strip was 1.5 mm, and they were further cut into pieces of 30 mm x 25 mm for the annealing tests. A hole with a diameter of 2 mm was drilled at the top of the sample to enable hanging in the furnace. Samples were cleaned with ethanol before annealing. The chemical composition of the steel is presented in **Table 1**.

Temperatures of 1100 ˚C, 1125 ˚C, 1150 ˚C, 1175 ˚C, and 1200 ˚C and exposure times of 1, 3, and 5 minutes were used for annealing. The chemical composition of the atmosphere (72.69% N_2, 16.1% H_2O, 8% CO_2, 3.22% O_2) simulated industrial furnace conditions when CH_4 with 20% excess air is used as fuel. In this study, the atmosphere was produced by mixing pressurized air, CO_2, N_2, and H_2O gases in a suitable ratio and feeding the mixture into the furnace at a gas flow rate of 2 l/min.

Laboratory annealing was performed in a vertical tube furnace under isothermal conditions. The furnace was equipped with a computer-controlled electric motor regulating the position of the sample in the furnace. Heating curves of the samples with pre-annealing, annealing, and cooling steps were produced by adjusting the vertical position of the samples in the furnace to simulate a temperature profile of final annealing in an industrial furnace. The temperature of the sample was measured with a thermocouple near the center of the sample's side that moved with the sample in the furnace (**Figure 1a**).

For each temperature used in this study, the vertical furnace temperature was measured from the center of the furnace to the top of it, first in 5 mm increments until a distance of 60 mm and then in 10 mm increments. The obtained vertical furnace temperature profile for a given temperature was used in calculating the required height for the sample in a given time-step to simulate the temperature profile of the industrial annealing furnace. In the pre-annealing step, the sample was heated with a higher heating rate for 45 s until the actual annealing zone began and the heating rate decreased. In the annealing step, the sample temperature was raised close to the isothermal temperature of the furnace during exposure time. Samples were cooled down in two sequential phases: first, the samples were cooled inside the furnace by lifting them away from the hot area, after which they were removed from the furnace and allowed to cool down to room temperature. A target heating curve of an annealed sample is presented in **Figure 2** with an exposure time of three minutes.

2.1. Electrolyte pickling

A neutral electrolyte pickling device was used to evaluate the pickling effectiveness. The device consisted of three parts, as shown in Figure 1b. The electrolyte solution of 17 wt-% sodium sulfate (Na_2SO_4, Honeywell, purity ≥99.0%) was heated to over 60 °C in an electrolyte tank with a volume of 2 l.

Pickling temperatures were monitored and are reported in the results. Electrolyte was circulated with a Watson Marlow 520DU (Watson-Marlow, United Kingdom) peristaltic pump using a flow rate of 800 ml/min between the pickling vessel and the electrolyte tank. The pickling vessel consisted of the PTFE vessel and lid, with the volume of the vessel being 0.4 l. Two grade 1 titanium electrodes with the same dimensions as the sample were connected to the lid and positioned around the sample in the middle of the vessel, as shown in Figure 1b. The distance between the electrodes and sample was 15 mm. The titanium electrodes acted as counter electrodes, while the sample acted as the working electrode. Keysight E36312A (Keysight, Malaysia) was used as the power source and to record the current and potential applied to the system. Pickling was done using the settings presented in **Table 2**. The pickled samples were lightly brushed with a toothbrush to remove loose scale and pickling sludge. Finally, brushed samples were dried by blowing with compressed air and stored for analysis.

2.3. Characterization

The annealed samples were mounted in resin, cut in half, and polished. Cross-sections of the samples were examined using FESEM (Sigma Ultra Plus) with an EDS point and map analyses to determine the structure and chemical composition of the oxide scale. Elemental analysis of the scale as a function of depth and scale thickness was analyzed via glow discharge optical emission spectroscopy (GDOES). The GDOES measurement was performed with a 2.5 mm diameter burn spot and 150 s analysis time. The thickness of the oxide scale was determined based on the oxygen content, and the interface between the oxide scale and base material was positioned at the point where the oxygen content dropped below 5 wt-%. [3,26,27]

The pickled samples were analyzed using FESEM backscatter images. Images with a magnification of 500x were taken from three parts of the sample, as shown in **Figure 3**. EDS was used to confirm the observed oxide and chromium depleted layers. In the FESEM images,

the chromium-depleted layer was generally observed as white and the oxide layers as ranging from light to dark grey. In samples where the oxide layer covered the whole surface, the coloration was inverse due to the contrast between the oxide mixture of white and grey pixels.

2.4. Analysis of FESEM images

Evaluation of the pickling effectiveness was carried out by means of image analysis. The FESEM images were 8-bit greyscale images, meaning that the intensity range is defined between 0 and 255. Since the phase of interest showed as white objects on a darker background, the images were segmented such that the objects of interest were mapped to a scaled intensity of 1 and the darker background to 0. Prior to segmentation, the images were treated with a Gaussian filter to reduce noise from the image, and thus to prevent oversegmentation.[28] The binarization threshold was chosen using Otsu's method. [29] The mapping rule for individual pixels *(x,y)* is then given in Equation (1):

$$u(x,y) = \begin{cases} 1, & if\ f(x,y) > T_b \\ 0, & if\ f(x,y)\ \leq T_b \end{cases}, \qquad (1)$$

where *u(x,y)* is the resulting binarized image, *f(x,y)* is the original image and T_b is the binarization threshold. After segmentation, the binarized images were treated with a binary morphological opening, which is defined as Equation (2)[30]:

$$A \circ B = (A \ominus B) \oplus B, \qquad (2)$$

where $\ominus$ is the erosion performed between the original image A and structuring element B, and $\oplus$ is the dilation performed between the eroded result and structuring element B. The morphological opening treats the image with a structure element such that it removes any objects smaller than the structure element from the image.[30] Consequently, if a sufficiently small white pixel structure element is used, then the morphological opening is expected to treat the image such that it removes the small white areas that cannot be reliably differentiated as the

object of interest, but only the areas formed because of the obscurity in the selection of the threshold. The obscurity arises from the noise, even though the images are pre-processed with a filter. Finally, the fraction of white pixels in the binarized and opened result image is given as Equation (3):

$$f_W = \frac{\sum_{y=1}^{L}\sum_{x=1}^{W} u(x,y)}{LW}, \qquad (3)$$

where *L* and *W* are the length and width of an image in terms of pixel count.

3. Results

3.1. Characterization of oxide scale

Thickness of the oxide scales was determined using GDOES. Influences of the annealing temperature and exposure time on oxide scale formation were studied from the cross sections of the samples with FESEM. EDS analyses were performed on FESEM images to determine the chemical composition of the oxide scales. The morphologies of oxides could be roughly divided into three categories: a chromium-rich oxide layer, a chromium-rich oxide layer with iron oxide nodules, and a layered oxide structure. The oxide scale's thickness (GDOES) and morphology (FESEM-EDS) are presented in **Table 3**.

EDS analysis of the chromium-rich oxide layer formed at the lowest annealing temperatures showed that the oxide layer also contained manganese, especially in the thicker oxide layers. An oxide scale formed at 1100 °C and an annealing time of five minutes is shown in **Figure 4a**, and the corresponding chemical composition determined with EDS point analysis is presented in **Table 4**. The composition of the oxide scale layer mainly consisted of chromium and other elements, namely iron, manganese, and silicon. The GDOES depth profile of the sample is presented in Figure 4b. The thickness of the oxide layer was 0.560 µm, and three sublayers

could be distinguished from it. The outer sublayer contained chromium and it was enriched in manganese and iron. The middle sublayer was a chromium-rich layer and its iron content increased towards the oxide-metal interface. The innermost sublayer was enriched in silicon. Of note, silicon oxide (SiO_2) formed both in the oxide-metal interface and inside the steel substrate (Figure 4c). Similar sublayers were also observed when studying the chromium-rich oxide layers formed under all annealing conditions.

GDOES depth profiles showed chromium-depleted layers below the chromium-oxide layers. The chromium content of the annealed surfaces at 1100 °C is shown in Figure 4d. The chromium-depleted layer extended deeper into the substrate steel as the annealing time increased. The chromium content stabilized after depletion at depths of approximately 1 µm, 3 µm, and 5 µm.

The formation of iron-rich nodules began as a result of higher temperatures and longer exposure times. An exposure time of five minutes at 1125 °C produced an oxide layer with a thickness of 0.600 µm. An example of an iron-rich oxide nodule that formed under such conditions is presented in **Figure 5a**. EDS maps showed that the outer part of the nodules consists of iron-rich oxide, while the onset of the expanding chromium rich internal oxidation occurred below the nodule. By increasing the temperature for the five-minute annealing process to 1150 °C, as shown in Figure 5c, a thicker oxide layer (0.925 µm) and larger oxide nodules with distinct internal oxidation formed below them. Below the iron-rich oxide nodule, the internal oxidation zone consisted of enriched iron and nickel areas. Similar large oxide nodules developed in under three minutes time at 1175 °C, as presented in Figure 5e. EDS point analysis proved that the outer part of the nodules consisted mainly of iron oxide (point 2 in Table 4), while the inner parts consisted of chromium and iron-rich spinel with low nickel enrichment.

The layered oxide structure began to form with an exposure time of five minutes at 1175 °C and of three minutes at 1200 °C, causing the thickness of the oxide scale to increase significantly. The large netlike oxide pockets that formed under the large iron-rich oxide nodules are presented in Figure 5f. The uneven surface of the outer iron-rich oxide is the result of fine pieces coming off after removing the steel samples from the furnace.

EDS point analysis showed that this outer oxide scale consisted almost completely of iron oxide (point 5 in Table 4). In point 6, the grey area close to the surface consisted of chromium and iron-rich spinel, while the lighter area analyzed in point 7 also included a high concentration of nickel. In addition to pockets, it is also possible for a two-layer scale structure to form under these conditions. The two-layer scale structure consists of an outer iron-rich layer and an inner netlike-structured scale layers.

Under the most demanding annealing condition, 1200 °C and five minutes, the formed oxide morphology was completely layered, as shown in Figure 5g. The FESEM image shows that the resulting netlike-structured oxide scale layer was quite thick, more than 30 µm. In addition, a thick layer of iron oxide had partially spalled off the surface after annealing. A closer inspection of the netlike scale structure is presented in Figure 5h. The outer, grey part of the structure consisted of iron and chromium-rich spinel (point 8 in Table 4). The image also shows that the amount of gray area decreases towards the oxide-metal interface, while amount of lighter gray area increases. In the lighter area, the oxygen content was low, indicating that the area was metallic and consisted of iron and a large amount of nickel. The black areas in the netlike structure are voids.

3.2. Pickling

The samples can be classified into four categories based on the extent of the oxide layer removal. Examples of each category can be seen in **Figure 6**. The category “excellent” includes samples

in which most of the oxide was removed during neutral electrolyte pickling. Samples with a low temperature and short annealing time fall under this category. Samples in the category denoting “good” pickling efficiency had roughly equal amounts of oxide-free areas and oxide-containing areas. During the final mixed-acid pickling phase, the remaining oxides are removed by undercutting, as the acid mixture dissolves the chromium-depleted layer. Most of the samples fall into this category. Samples classified as “decent” results remained mostly covered in the oxide layer. In these samples, mixed-acid pickling is hindered by the remaining oxide layer. Bad results included samples covered by an oxide layer even after pickling. In a test run with a double-neutral electrolytic pickling time, the sample was left unevenly pickled, with a large portion of the sample covered under a thick oxide layer, while others were pickled bright. Since the contrast in oxides in the FESEM images shift from unified gray to a mixture of gray and white, an inversion of colors was required before the pixel histogram analysis of the samples classified as bad. Long temperatures and annealing times are prominent species in the final category.

The results of the picture-by-picture evaluation are summarized in **Table 5**, which shows the total number of categorized images in each of the categories. A score ranging from 4 to 1 was given to each image, and an average score was calculated for each temperature-time combination.

4. Discussion

4.1. Morphology progression

Annealing temperature and exposure time have a clear effect on the formed scale morphology of AISI 304 steel in the water vapor-containing atmosphere. A variation of 100 ˚C in the annealing temperature can cause significant difference in the oxide scale. Samples annealed for one minute at all tested temperatures showed the formation of a chromium-rich oxide layer,

with the oxide layers differing in their thicknesses and amounts of iron enrichment. A far more dramatic difference was observed when the annealing time was increased to five minutes: the morphology of oxide scales changed from the thin, chromium-rich oxide layer at 1100 ˚C to a thick layered scale structure at 1200 ˚C. Previous studies have also detected strong effects between annealing time and temperature as well as scale formation.[14,31]

By changing the annealing conditions to a higher temperature and longer exposure time, the formed scale structures appeared in the following order: a chromium-oxide layer, a chromium-oxide layer with iron-rich oxide nodules, and a layered oxide structure. The chromium-oxide layer forms when chromium diffuses towards the gas-metal interface and oxidizes, and that diffusion causes a chromium-depleted zone to form below the oxide layer in the steel substrate. The chromium-oxide layer is called protective due to the weak diffusion of gas and metal atoms through it.[1] However, iron ends up in the gas-oxide interface via the chromium-oxide layer either by diffusion or cracks when annealing continues [32], and oxidized iron forms nodules on the surface of the Cr_2O_3 layer.

The morphology of the oxide-scale layer develops from the formation of initially small iron oxide nodules, followed by internal chromium oxidation, and then the formation of netlike structured pockets below the nodules. Internal oxidation below the iron-rich oxide nodules begins after the chromium concentration decreases to a critical value at the oxide-metal interface, prohibiting the formation of a continuous external oxide layer.[17] In the internal oxidation process, the oxidation of chromium and iron forms $(Fe,Cr)_xO_y$ spinels due to the inward diffusion of oxygen[32], while non-oxidized nickel and iron-rich areas remain in the spinel structure, forming an internal, net-like scale structure. Zeng et al.[33] proposed that the outward diffusion of chromium and iron atoms through the net-like structure occurs via a network of Fe- and Ni-rich particles and the inward diffusion of oxygen via the oxidized area network.

The FESEM results presented in Figure 5g show that when a thick, iron-rich oxide layer cracked and spalled from the surface, new iron-rich oxide formed on the surface of the spinel layer. The formation of iron oxide was the result of a higher oxidation rate of iron than that of chromium at the gas-spinel interface due to the higher mobility of iron ions in the spinel structure towards the surface.[1]

Based on morphology results, it is important to recognize the impact of the exceptional industrial steel annealing conditions on scaling behavior. Minor oxide scale formation as chromium oxide layer is an advantageous in terms of controlling material loss. Internal oxidation below the iron-rich oxide nodules may cause surface imperfections after pickling processes due to penetration depth and unevenness of oxidation into stainless steel matrix. Additionally, spalling and rapid formation of iron oxide layer on the surface of net-like scale structure contribute to material loss during the annealing process, and greater amounts of scale may cause problems in pickling.

The morphology progression of the oxide-scale layer was also observed through changes in the chromium content related to depth. The depth profiles of the chromium content for samples annealed for five minutes are presented in **Figure 7**. Samples at 1100 ˚C and 1125 ˚C had similar curves for chromium content due to their similar morphology and scale thickness. Comparing 1150 ˚C to the lowest temperature, the chromium content peak was deeper due to the thicker oxide-scale layer. Clearly, the elevated Cr content at 1100 ˚C and 1125 ˚C was the result of a chromium-rich oxide layer that had formed on the surface of the samples. The highest chromium content ranged from 40 to 57 wt-% in the GDOES results for all chromium-oxide layers. However, neither annealing temperature nor time dependence were observed for the chromium content, which may be the result of measurement uncertainty close to the gas-oxide interface. A more accurate comparison of the chromium content in the oxide layer requires further research. The breakaway oxidation observed for samples at 1175 ˚C and 1200 ˚C

resulted in totally different chromium content curves, where the chromium content of the gas-oxide interface in the iron-oxide layer was low and the content increased with the transition to the spinel-containing layer.

4.2. Effect of annealing temperature and time on thicknesses of oxide scale and chromium-depleted layer

Annealing temperature and time affect the thickness of the oxide-scale layer (**Figure 8**). Oxide scales mainly consisting of thin, chromium-rich oxides layers are more dependent on time than temperature when looking at oxide thicknesses. At 1100 °C, the oxide thickness was determined to be only 0.165 µm after an annealing time of one minute, and the thickness more than tripled by increasing the annealing time to five minutes (0.560 µm). However, the thicknesses of the scales increased by only 2.5 times, from 0.165 µm to 0.415 µm, when using a one-minute annealing time and increasing the temperature from 1100 ˚C to 1200 ℃.

A much greater difference in the thicknesses of the scales was detected with longer exposure times. When looking at annealed samples for five minutes, the scale thickness increased from 0,560 µm to over 30 µm as the temperature increased from 1100 ˚C to 1200 ˚C. The observed development in the thickness of the scale can be explained by a change in the morphology of the scales from the chromium-rich oxide layer to the layered scale structure resulting from breakaway oxidation.

At longer annealing times and at higher temperatures, the scale is less homogeneous due to changes in the morphology and spalling-oxide scale from the surface. Thus, the measured thicknesses do not represent the entire surface of the sample as well as they do for the thin, chromium-oxide layer. For example, the thickness of the sample annealed for three minutes at 1200 ˚C was only 1.81 µm, differing significantly from the estimate obtained from the FESEM

images and from the sample annealed for five minutes at 1175 ˚C with a corresponding scale morphology (thickness 7.025 µm).

Furthermore, the annealing conditions affect the formed chromium-depleted zone. At an annealing time of one minute, temperatures cause the chromium-depleted layer to extend from about 1 µm to 2 µm. The thickness of the Cr-depleted layer increased significantly with increasing annealing time. Even at the lowest annealing temperature for five minutes, the Cr -depleted layer already extended to 5 µm. Therefore, shorter annealing times should be preferred to keep the Cr-depleted zone as thin as possible so that less surface material needs to be removed by pickling. Final removal of the chromium-depleted layer from the surface of stainless steel is usually done via a mixed acid bath after electrolytic pickling,[3] and therefore, the removal of the Cr-depleted layer was not studied in this work.

4.3. Effect of oxide scale on pickling efficiency

After the initial drop in pickling excellency, the most significant loss in pickling efficiency occurred at 1175 °C with an annealing time of five minutes and at 1200 °C for three minutes onwards (Table 5). Since chromium-oxide dissolution is the main mechanism in neutral electrolyte pickling, samples in which the majority of the oxide layer was composed of chromium oxide generally exhibited excellent or good pickling results, depending on the thickness of the oxide layer.

As the annealing temperature and time increased, iron oxide formed. The dissolution of iron oxide is slow, and thus, the pickling results worsened significantly at higher temperatures and annealing times. At first, however, iron oxides are present as iron oxide nodules. The majority of the oxide layer remains easy-to-pickle, and the pickling results are categorized as good despite of the nodules. As the number of iron-oxide nodules increased, however, the area

unaffected by neutral electrolytic pickling increased, leading to ever-decreasing pickling efficiency. At the highest temperatures and annealing times studied, the iron-oxide formation had reached the exponential phase, and dissolution of chromium oxide via neutral electrolytic pickling was hindered considerably. A study by Li et al.[34] suggests that for such samples, the most efficient mechanism had changed from the dissolution of chromium oxide to the under-cutting of oxide by dissolution of the metallic nickel and iron at the oxide–metal phase boundary.

As noted by Hildén et al. [35] the scale thickness predicts the quantity of the electricity required to dissolve the oxide layer, hence the benefits of the extended pickling for the samples with a thicker oxide layer. However, the potential required to drive the dissolution reaction is increased. During a test run at double pickling, carried out with a sample annealed in 1175 ˚C for 5 min, the dissolution of the oxide layer improved visibly. However, the results were uneven, suggesting an increased risk of product surface defects as the unevenness could affect the results of mixed acid pickling.

According on the results, the annealing of stainless steel can be done at high temperatures without compromising pickling effectivity if the annealing time is kept short enough and the amount of the iron-oxide nodules remains low while the chromium-oxide area remains high. Likewise, the pickling procedure should be altered for samples that have reached the phase of exponential iron oxide growth.

To study the effect of annealing conditions on the pickling result, a multiple linear regression model was fitted to an averaged fraction of white pixels in binarized images calculated for each of the experimental conditions. Prior to the fit, the data was standardized ($\mu = 0;\ \sigma^2 = 1$) to compare the magnitude of effects. The details of the explanatory model are given in **Table 6.** The table shows that the model estimates are reliable, and consequently, there is a small risk of rejecting the null hypothesis when considering the effects of explanatory variables on the

fraction of white pixels in the segmented image. However, as seen from the figures of merit for the model fitted for the full set of images, there is variance between the fraction of white pixels in the segmented image acquired from the sample treated with the same experimental conditions. This is because the surface of a single sample is not thoroughly homogeneous. This fact supports a quality assessment procedure in which a set of several images is taken from a single metallographic sample and then the image features are averaged over the sample images. It should be noted that the data does not follow the assumptions of normality, and hence, the standard error estimates (SE) may be underestimated, meaning that the estimate of the confidence region is not as accurate as it would be for a larger dataset. Still, the explanatory power of the model can be considered relatively good, as the logistic transformation of the time and temperature account for the majority of variance in the fraction of white areas in all the studied images. In **Table 7**, the corresponding means and standard deviations for the white pixel fractions are presented. From the table it can be seen that both the temperature and exposure time for annealing have an observable effect on the fraction of white pixels obtained with segmentation. It should be noted that the estimates are not biased because of image analysis treatment method itself, as the procedure was the same for all analyzed samples. However, it would be beneficial to have more data to better identify the effects of scale compositions on the results. More data would also allow for a more detailed segmentation of the image, for example with respect to defect groups and morphologically different scales. For the present dataset, only the variance in the white area can be analyzed reliably, as the type of scale has an interaction effect with the original design variables. However, identifying additional effects is a matter for future studies.

The dependence of the whiteness of the pickled surface on annealing time and temperature based on the descaling effectiveness model is presented in **Figure 9**. The proposed linear regression model with a logistic transform and interaction term can explain the fractions of

white pixels (f_w) in the segmented image. For example, conditions at 1200 °C for five minutes produced a thick-layered scale and, after pickling, no white, oxide-free areas formed. Therefore, the pickling result of the sample should be discontinuous due to changes in the scale type. Consequently, a partially defined model with dichotomized effects concerning the type of scale would be a more precise approximation of the sample's true behavior.

Based on the model, increasing both the annealing temperature and the exposure time impairs the pickling result. When comparing the annealing temperatures of 1100 °C and 1150 °C based on whiteness, the exposure time had a slightly greater effect on the pickling result at the lower temperature. The greater change is due to the achievement of an almost clean surface by pickling from the oxide with the shortest annealing time whereby the pickling result curve becomes sharper. The graph shows that the sample at 1100 °C with a five-minute annealing time had a better pickling efficiency than the sample at 1200 °C with a one-minute annealing time, despite the greater oxide scale thickness of the first mentioned sample. Thus, scale thickness is not the most significant factor when considering the pickling efficiency of the oxide scale; the more important factors seem to be scale morphology and elemental composition.

Previous studies have shown that the pickling of the chromium-rich oxide layer is affected by the composition of the layer. Similar sublayers are detected in this study as well: an outer Mn- and Cr-rich layer, a middle chromium-rich layer with iron content, and an Si-rich layer at the oxide-metal interface. Hildén et al.[36] have observed a three-step dissolution mechanism for the chromium-rich oxide layer in neutral electrolyte pickling, the steps of which are the result of these chromium-rich oxide sublayers. In this study, enrichment of manganese was observed at each chromium-rich oxide layer that had formed, regardless of annealing conditions. Chromium- and manganese-rich oxide is known to be highly soluble in electrolyte pickling, and Fernando et al.[25] have demonstrated that the pickling of the chromium-oxide layer is easier with a manganese-rich outer layer. Dissolution of silicon oxide is much weaker than that of

chromium or manganese, so it complicates the pickling process, using HF required for pickling.[25] Minimizing the formation of silicon oxide during annealing is thus beneficial for the efficiency of the electrolyte pickling process. The elemental composition of the chromium-oxide layer requires further research so that the effect of different annealing conditions on the composition of oxide can be compared to pickling efficiency.

In summary, changes in oxide scale formation caused by annealing time appear to have a greater effect on the success of the electrolytic pickling results according to both categorization and pickling model. When short exposure time is used, the morphology of the oxide scale remains mainly as chromium-rich oxide layer and the chromium depleted layer as thin as possible. Oxidation is the byproduct from the primary function of steel annealing: achieving the target grain size. However, optimization of grain size in tandem with pickling efficiency is beyond the scope of this paper and would require more research.

5. Conclusions

The short-term annealing of AISI 304 stainless steel in a humid atmosphere between 1100 and 1200 °C in 25 °C intervals and the effects of the resulting oxide scale on neutral electrolyte pickling efficiency were studied. Exceptional conditions during industrial steel annealing significantly affect the oxidation of the steel surface and the following results were obtained:

- Shorter annealing times should be preferred when aiming for a thin chromium-rich oxide layer and to keep the Cr-depleted zone as thin as possible. Thus, the material loss during the subsequent pickling process would remain minor.
- For longer annealing times, internal oxidation below iron-rich oxide nodules is formed and this can cause surface imperfections. In addition, a thick iron-containing scale layer causes difficulty in electrolytic pickling process.

- The efficiency of neutral electrolyte pickling is not significantly reduced if the exposure time of high-temperature annealing is kept sufficiency low. During critical conditions, 1175 °C with a five-minute annealing time and 1200 °C with three minutes, the thickness of the oxide scale begins to increase significantly, which directly reflects as a decrease in pickling efficiency.
- The development of pickling efficiency model is able to predict well-observed pickling results so long as the oxide-free areas are present in the analyzed images of the pickled surfaces. When comparing the electrolytic pickling efficiency of the mainly chromium-rich oxide layers with the model, it was found that the proportion of white pixels decreases even more at 1100 °C than at 1150 °C regarding exposure time due to especially better pickling result at the shortest annealing time.

Acknowledgements

This research was funded as part of the Business Finland Symbiosis of Metals Production and Nature project (SYMMET). Acknowledgements are expressed to the research staff of Outokumpu Stainless Ltd.'s Tornio works for supplying the materials used in this study.

Received: ((will be filled in by the editorial staff))
Revised: ((will be filled in by the editorial staff))
Published online: ((will be filled in by the editorial staff))

References

[1] A.Visnapuu, J. S. Volosin, R.B. Schluter, *United States Department of Interior*. *Report of Investigations*, **1994**, *RI 9491*.

[2] S. Gonzales, L. Combarmond, M. T. Tran, Y. Wouters, A. Galerie, *Mater. Sci. Forum*. **2008**, *595-598*, 601.

[3] D. Lindell, R. Pettersson, *Steel Research Int*. **2010**, *81*, 542.

[4] N. Karimi, F. Riffard, F. Rabaste, S. Perrier, R. Cueff, C. Issartel, H. Buscail, *Appl. Surf. Sci.* **2008**, *254*, 2292.

[5] A. C. S. Sabioni, A.-M. Huntz, E. C. da Luz, M. Mantel, C. Haut, *Mater. Res*. **2003**, *6*, 179.

[6] A. M. Huntz, A. Reckmann, C. Haut, C. Sévérac, M. Herbst, F.C.T. Resende, A. C. S. Sabioni, *Mater. Sci. Eng. A*. **2007**, *447*, 266.

[7] C. Pascal, M Braccini, V. Parry, E. Fedorova, M. Mantel, D. Oquab, D. Monceau, *Mater. Charact*. **2017**, *127*, 161.

[8] W. Liu, *Eng. Fail. Anal*. **2016**, *70*, 419.

[9] S. G. Wang, M. Sun, H. B. Han, K. Long, Z. D. Zhang, *Corros. Sci*. **2013**, *72*, 64.

[10] K. A. Habib, M. S. Damra, J. J. Saura, I. Cervera, J. Bell´es, *Int. J. Corros*. **2011**, 2011.

[11] A. Col, V. Parry, C. Pascal, *Corros. Sci*, **2017**, *114*, 17.

[12] V. Parry, A. Col, C. Pascal, Corros. Sci, **2019**, *160*, 108149.

[13] N. Zacchetti, S. Bellini, A. Adrover, M. Giona, *Mater. High Temp*. **2009**, *26*, 31.

[14] C. E. R. de Carvalho, G. M. da Costa, A. B. Cota, E. D. Rossi, *Mater. Res*. **2006**, *9*, 393.

[15] H. Asteman, J.-E. Svensson, M. Norell, L.-G. Johansson, *Oxid. Metals*. **2000**, *54*, 11.

[16] V. Badin, E. Diamanti, P. Forêt. E. Darque-Ceretti, *Procedia Mater. Sci*. **2015**, *9*, 48.

[17] S.-Y. Cheng, S.-L. Kuan, W.-T. Tsai, *Corros. Sci*. **2006**, *48*, 634.

[18] C. Strauß, R. Gustus, W. Maus-Friedrichs, S. Schöler, U. Holländer, K. Möhwald, *J. Mater. Process*. **2019**, *264*, 1.

[19] N. Ohta, F. Yanagishima, T. Kaihara, A. Kishida, K. Sato, M. Ochiai, *US 4713154A*, **1987**.

[20] B. Ozturk, R. Matway, *ISIJ Int*. **1997**, *37*, 169.

[21] Q. Jin, J. Li, Y. Xu, X. Xiao, W. Zhang, L. Jiang, *Corros. Sci*. **2010**, *52*, 2846.

[22] X. Cheng, Z. Jiang, D. Wei, J. Zhao, B. J. Monaghan, R. J. Longbottom, L. Jiang, *Surf. Coat. Tech*. **2014**, *258*, 257.

[23] J. Issartel, S. Martoia, F. Charlot, V. Parry, Y. Wouters, A. Galerie, *Mater. at High Temp*. **2011**, *28*, 274.

[24] D. Lindell, T. Ekman, R. Pettersson, *Steel Res. Int*. **2015**, *86*, 557.

[25] L. A. Fernando, D. R. Zaremski, *Metall. Trans*. **1988**, *19A*, 1083.

[26] N. Ipek, B. Holm, R. Pettersson, G. Runnsjö, M. Karlsson, *Mater. Corros*. **2005**, *56*, 521.

[27] R. Elger, R. Pettersson, *Oxid. Met*. **2014**, *82*, 469.

[28] P. Getreuer, *Image Processing On Line*. **2013**, *3*, 286.

[29] N. Otsu, *IEEE Trans. Syst., Man, Cybern*. **1979**, *9*, 62.

[30] R. M. Haralick, S. R. Sternberg, X. Zhuang, *IEEE Trans. Pattern Anal. Machine Intell*. **1987**, *4*, 532.

[31] X. Cheng, Z. Jiang, D. Wei, B. J. Monaghan, R. J. Longbottom, L. Jiang, *Met. Mater. Int*. **2015**, *21*, 251.

[32] J.-H. Kim, D.-I. Kim, S. Suwas, E. Fleury, K.-W. Yi, *Oxid. Met*. **2013**, *79*, 239.

[33] Z. Zeng, K. Natesan, Z. Cai, R. Cook, J. Hiller, *J. Mater. Eng. Perf*. **2014**, *23*, 1247.

[34] L.-F. Li, P. Caenen, M.-F. Jiang, *Corros. Sci*, **2008**, *50*, 2824.

[35] J. M. K. Hildén, J. V. A. Virtanen, R. L. K. Ruoppa, *Mater. Corros*. **2000**, *51*, 728.

[36] J. Hildén, J. Virtanen, O. Forsén, J. Aromaa, *Electrochim. Acta*. **2001**, *46*, 3859.

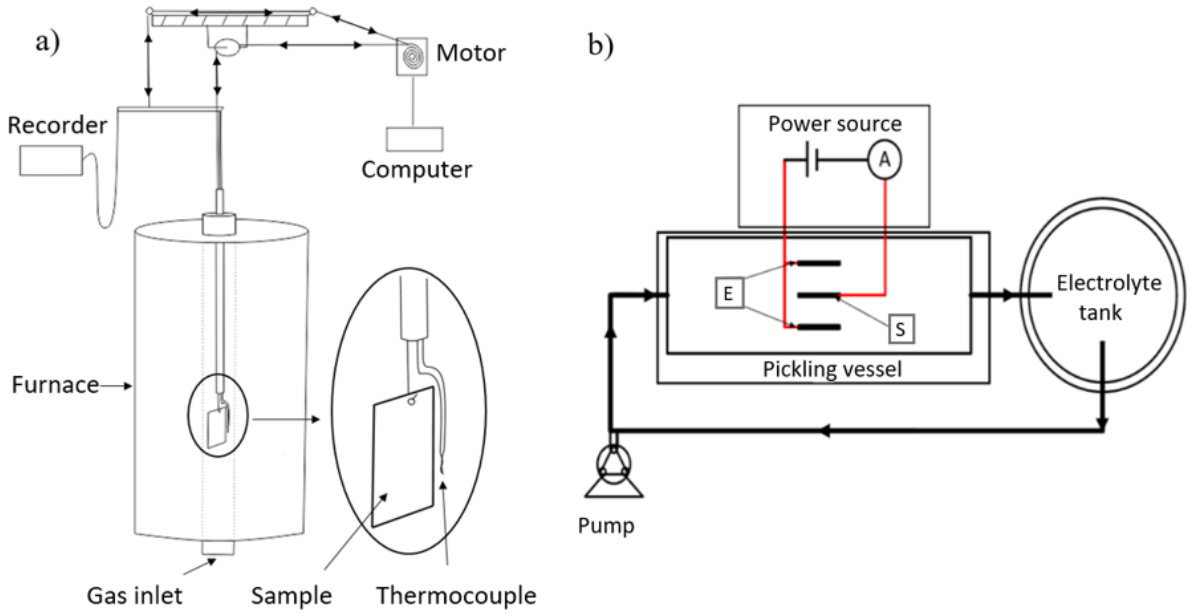

Figure 1. Schematic diagrams of laboratory devices: a) annealing device and temperature measurement with thermocouple, with b) pickling device: peristaltic pump circulates electrolytes (arrows) from the electrolyte tank to pickling vessel; in the pickling vessel, two electrodes (E) surround the sample (S) and the applied current and voltage are measured with power source (A).

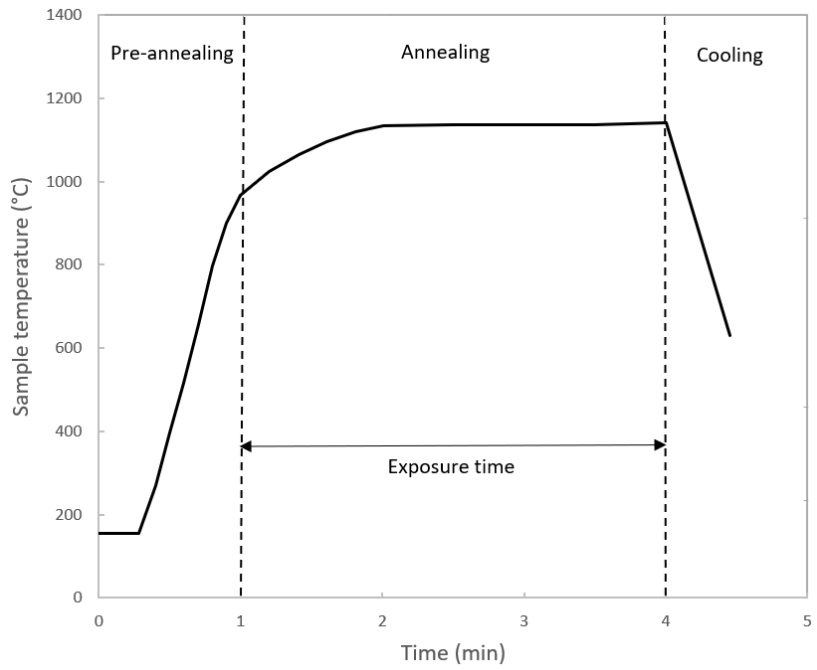

Figure 2. Target heating curve of the sample annealed at 1150 °C and three minutes.

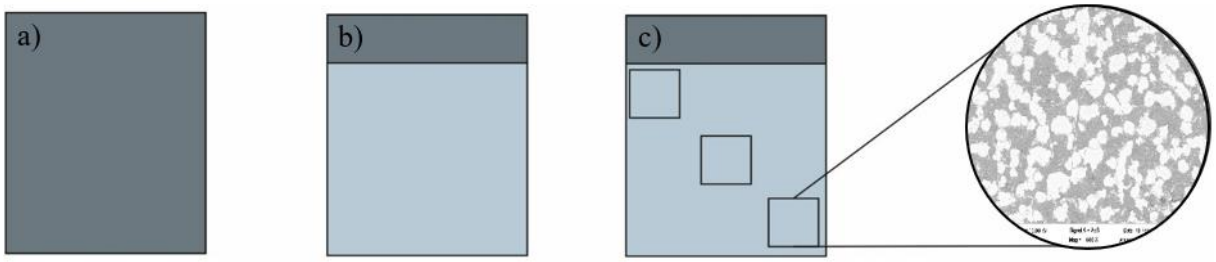

Figure 3. Research scheme for pickling effectiveness: a) samples are cut and annealed, b) samples are pickled in a neutral electrolyte, c) samples are characterized with FESEM-EDS from three different positions along the sample; the observed phases are classified as oxides or chromium-depleted metal layers by EDS analysis.

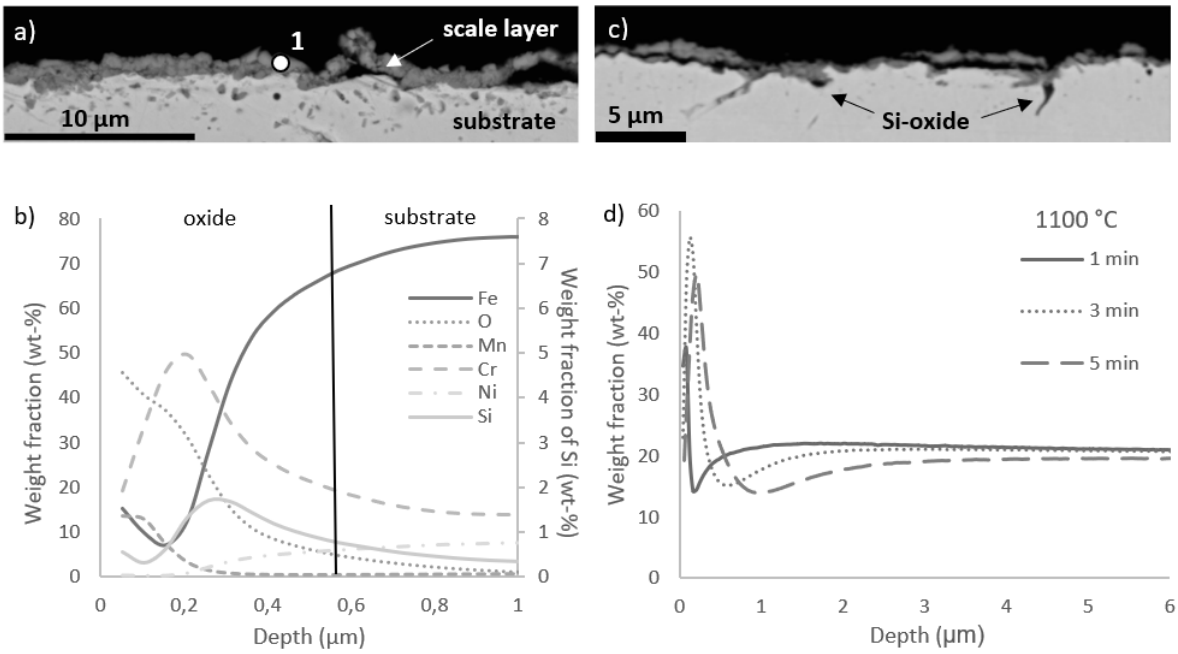

Figure 4. a) Chromium-rich oxide layer on the surface of the sample 1100 °C / 5 min, b) GDOES depth profile of sample at 1100 °C / 5 min, with the vertical line denoting the oxide-metal interface location, c) silicon oxide occurred as dark areas near the oxide-metal interface in the FESEM images, d) chromium-depleted layer thickness with different annealing times.

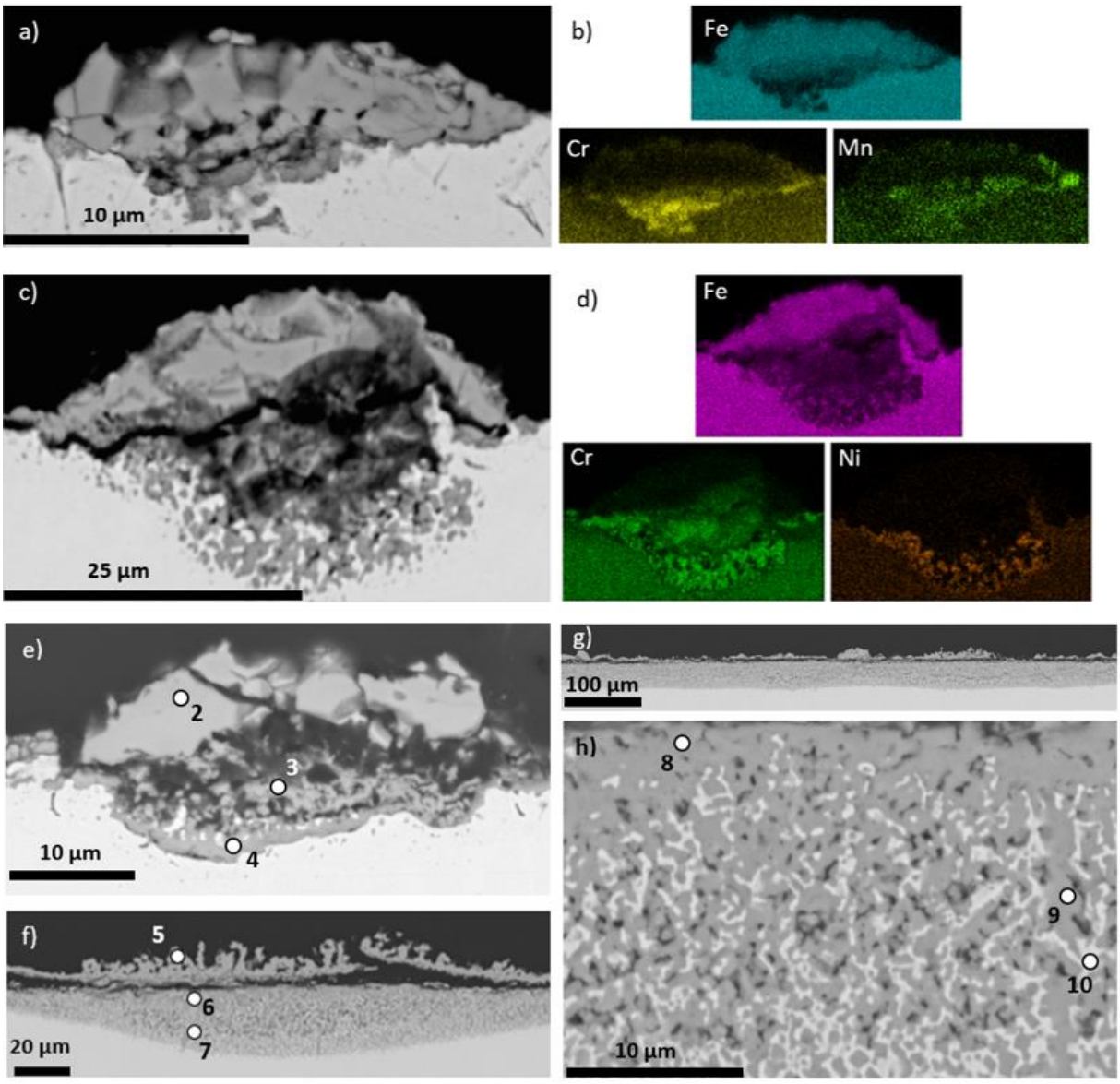

Figure 5. Scale structures and EDS analysis: a) iron-rich oxide nodule at 1125 °C / 5 min and b) EDS maps of the elements Fe, Cr, and Mn, c) iron-rich oxide nodule with internal oxidation at 1150 °C / 5 min and d) EDS maps of the element Fe, Cr, and Ni, e) iron-rich oxide nodule at 1175 °C / 3 min, f) iron oxide above a netlike oxide pocket at 1175 °C / 5 min, g) layered oxide structure: inner netlike scale layer and outer iron-rich scale layer at 1200 °C / 5 min, h) netlike scale structure at 1200 °C / 5 min.

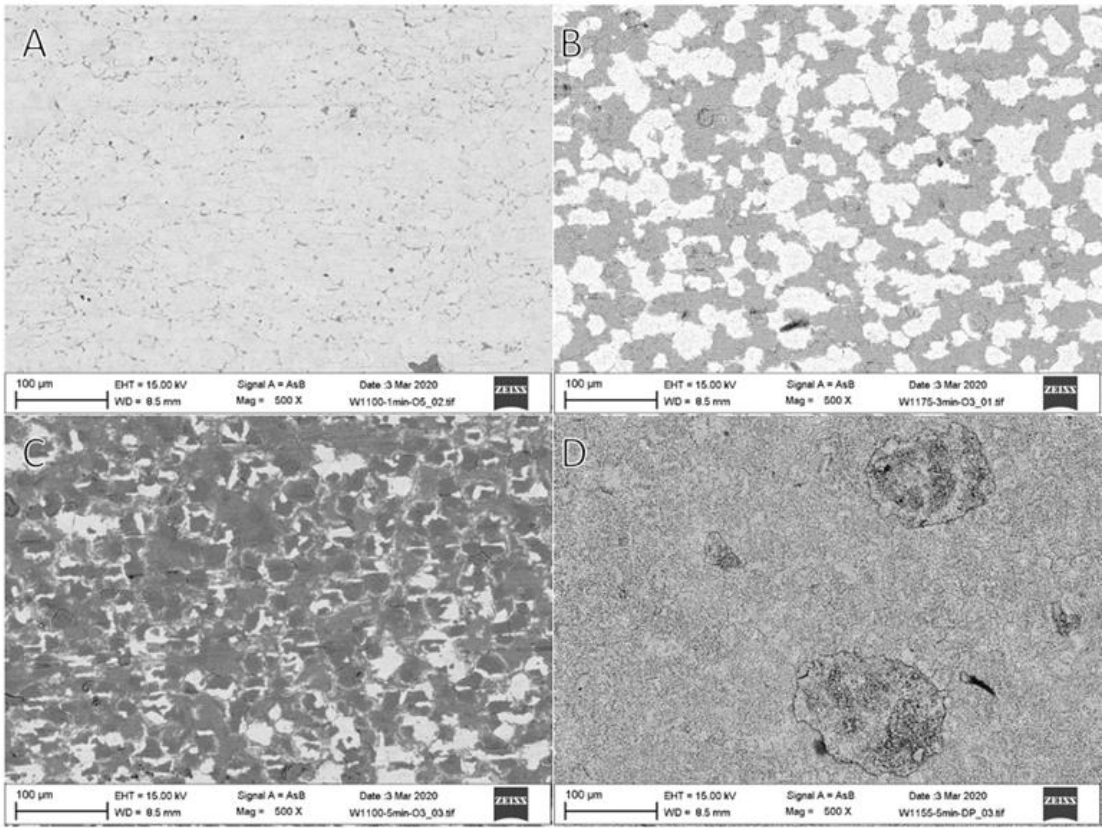

Figure 6. FESEM image of typical pickling examples grouped into each category: a) an excellent result, b) a good result, c) a decent result, d) a bad result. In subfigures A-C, the darker areas show the presence of oxides, as confirmed by EDS analysis, with the lighter areas being oxide free. In subfigure D, the sample is covered with oxides.

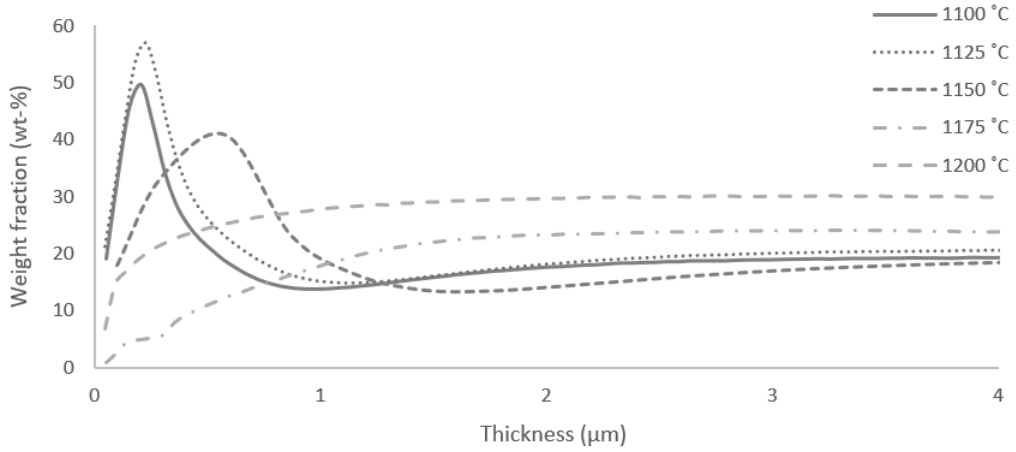

Figure 7. Depth variation in chromium content in the oxide scale after five minutes of annealing, in wt-%.

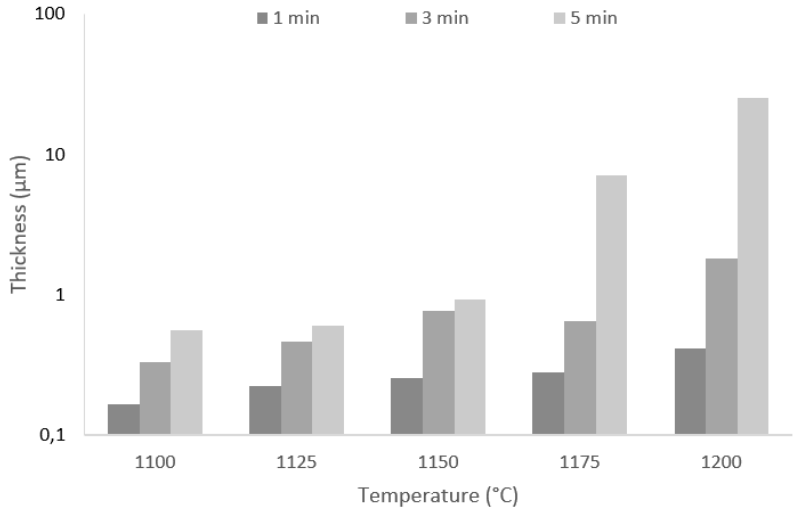

Figure 8. Thickness of oxide scales in terms of annealing temperature and time.

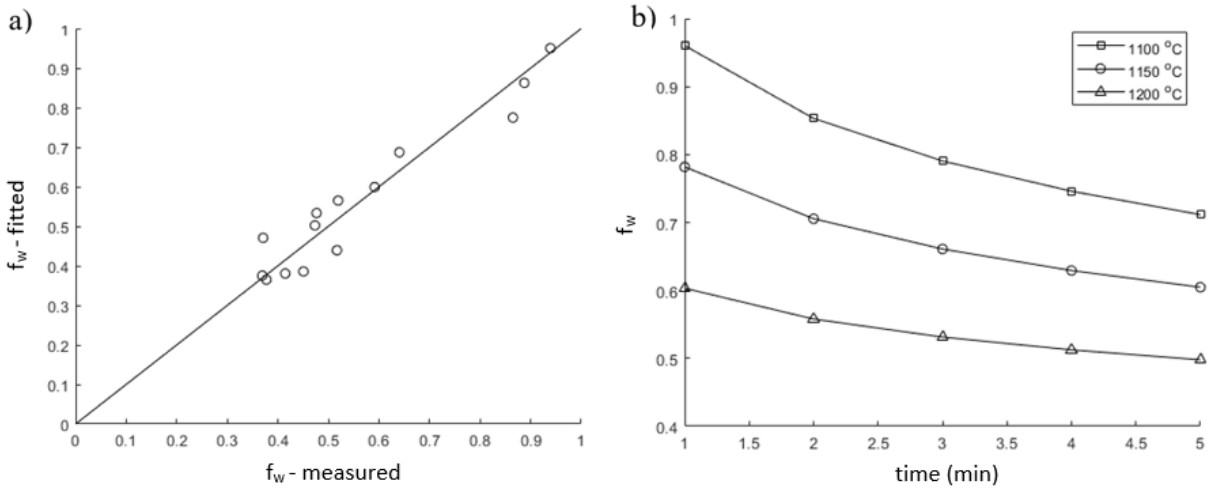

Figure 9. a) Measured vs. fitted fractions of white pixels in segmented images, b) responses to temperature and time for the model fitted to full data set.

Table 1. Chemical composition of AISI 304 stainless steel (wt-%)

Steel	**C**	**Cr**	**Ni**	**Mn_{max}**	**Si_{max}**	**Fe**
304	0.04	18.1	8.1	2	1	Bal.

Table 2. Applied potentiostatic voltage and galvanostatic current. During polarization switching, a 5 s zero current pause was applied to enable manual switching, whereas between the anodic pulses a 1 s pause was applied

Static	Time (s)	Applied voltage* (V)/current (A)	Sample polarization
Potentio	5	4*	Cathodic
Galvano	10	0.8	Anodic
Galvano	10	0.8	Anodic
Galvano	10	0.8	Anodic
Galvano	10	0.8	Anodic

Table 3. Oxide scale layers' thickness and morphological properties

T [°C]	**t [min]**	**Thickness [µm]**	**Properties**
1100	1	0.165	Cr_2O_3
	3	0.330	Cr_2O_3
	5	0.560	Cr_2O_3
1125	1	0.225	Cr_2O_3
	3	0.465	Cr_2O_3, few Fe-rich oxide nodules
	5	0.600	Cr_2O_3, Fe-rich oxide nodules
1150	1	0.255	Cr_2O_3
	3	0.775	Cr_2O_3, Fe-rich oxide nodules
	5	0.925	Cr_2O_3, large Fe-rich oxide nodules with inner oxidation
1175	1	0.280	Cr_2O_3, Fe-rich oxide nodules
	3	0.645	Cr_2O_3, large Fe-rich oxide nodules with inner oxidation
	5	7.025	Large netlike scale pockets under the large iron-rich oxide nodules or layered oxide structure
1200	1	0.415	Cr_2O_3, Fe-rich oxide nodules
	3	1.810	Large netlike scale pockets under the large iron-rich oxide nodules or layered oxide structure
	5	>30.0*	Layered oxide structure: Outer Fe-oxide layer and inner netlike Fe-Cr-spinel layer with metal particles (Fe, Ni).

*FESEM

Table 4. EDS point analysis of elements in the points marked 1–10 in the FESEM images, in wt-%

Point	**Fe**	**Cr**	**Ni**	**O**	**Si**	**Mn**	**Tot.**
1	9.27	56.66		30.53	0.19	1.79	98.44
2	69.61	2.51		25.04			97.16
3	22.26	43.09	3.5	26.25			95.10
4	20.59	48.56	1.39	28.14	0.43	2.37	101.49

5	66.73	2.34		25.88	1.46	96.41
6	47.47	20.31		31.69	0.87	100.34
7	54.33	15.68	19.07	15.31	0.74	105.12
8	41.45	29.79		30.98		102.22
9	30.76	39.84		27.73		98.34
10	56.20	7.91	33.18	5.98		103.28

Table 5. FESEM images classified into different categories and the corresponding score of the annealing condition. The categories "excellent," "good," "decent," and "bad" correspond to the score values ranging from 4 to 1 in ascending order

Temp/Time	Excellent	Good	Decent	Bad	Average grade	Average pickling temperature
1100 °C/1 min	9				4	61.0
1100 °C/3 min		5	1		2.83	65.4
1100 °C/5 min		8	1		2.89	61.0
1125 °C/1 min	6				4	60.7
1125 °C/3 min		6			3	59.7
1125 °C/5 min		6			3	60.2
1150 °C/1 min	9				4	60.5
1150 °C/3 min		5	1		2.83	60.1
1150 °C/5 min		4	1	1	2.5	60.1
1175 °C/1 min	3	3			3.5	61.7
1175 °C/3 min		4	2		2.67	62.1
1175 °C/5 min				3	1	62.0
1200 °C/1 min	3	9			3.25	60.3
1200 °C/3 min		1	3	2	1.83	62.4
1200 °C/5 min				6	1	61.9
1175 °C/5 min*		1		2	1.67	61.9

*pickled twice

Table 6. Standardized model of coefficient estimates with corresponding standard errors and t-test statistics for averaged values and for all images.

	Variable	Coefficient	SE	t-value	p-value	R^2	RMSE
Averaged	-	0.56	0.02	33.96	$1.21 \cdot 10^{-11}$	0.92	0.06
	T_b	-0.13	0.03	-4.60	$1.0 \cdot 10^{-3}$		
	log(t)	-1.81	0.55	-3.28	$8.0 \cdot 10^{-3}$		
	T·log(t)	1.63	0.55	2.96	$1.4 \cdot 10^{-3}$		

Full set	-	0.59	0.014	43.3	$8.25 \cdot 10^{-57}$	0.69	0.13
	T_b	-0.13	0.02	-6.44	$8.67 \cdot 10^{-9}$		
	log(t)	-1.77	0.45	-3.94	$1.75 \cdot 10^{-4}$		
	T·log(t)	1.58	0.45	3.54	$6.6 \cdot 10^{-4}$		

Table 7. Mean fractions of white pixels in the segmented images with corresponding standard deviations presented for each experimental condition.

Temperature (°C)	Time (min)		
	1	3	5
1100	0.94 ± 0.02	0.52 ± 0.13	0.45 ± 0.13
1125	0.89 ± 0.05	0.49 ± 0.10	0.41 ± 0.04
1150	0.87 ± 0.05	0.47 ± 0.01	0.37 ± 0.03
1175	0.64 ± 0.15	-	0.37 ± 0.07
1200	0.59 ± 0.23	0.51 ± 0.07	0.37 ± 0.17